

The Fingertip Manipulability Assessment of Tendon-driven Multi-fingered Hands

Junnan Li¹, Amartya Ganguly¹, Luis F. C. Figueredo^{1,2}, and Sami Haddadin¹

Author's Accepted Manuscript. Released under the Creative Commons license:

Attribution 4.0 International (CC BY 4.0) <https://creativecommons.org/licenses/by/4.0/>

Abstract—The ability of robotic fingers to exert force and exhibit motion is vital for achieving dexterity in manipulation tasks. To evaluate dexterous capabilities in terms of both features, i.e., quantifying finger performance that facilitates task planning and design optimization, we introduce the Fingertip Manipulability (FtM) metric. The FtM is a comprehensive assessment tool linked to finger parameters rather than specific task requirements, e.g., wrench information, contact-points, among others. It takes into account the entire voxelized fingertip workspace of all fingers, filling a gap in providing a global representation during the design and deployment phase of tendon-driven robotic hands. It composes the assessment map of a multi-fingered hand that enables real-time performance monitoring and planning for dexterous tendon-driven hands. To illustrate the practical application of this metric, we showcase its assessment of the Shadow Hand, demonstrating its characteristics in optimizing poses for a multi-finger grasping scenario.

Index Terms—Multifingered hands, Grasping, Performance Evaluation and Benchmarking, Manipulation Planning

I. INTRODUCTION

ADOPTION of multi-fingered robotic hands is on the rise with the goal of performing intricate multipurpose manipulation tasks like humans. Achieving such a milestone hinges on the ability to evaluate the quality of manipulation, which is typically assessed in terms of two key aspects: object stability [1] which quantifies how effectively a grasp can maintain the immobility of the object when subjected to external forces, while manipulability [2] gauges the capacity of the hand or fingers to change the position as well as the orientation of objects they are in contact with, based on the study by Yoshikawa et al.[3].

Algebraic grasping metrics assess the grasp quality of a hand in terms of contact information and hand configuration, [2], [4]–[6]. These methods are designed to evaluate task-specific situations, usually, defined through contact positions, wrench information, and/or grasp matrix associated with a desired graspable object. The extensive literature on grasp-wrench metrics reflects the challenges and application of such methods [2], [4]–[11]. Among existing studies, it is worth highlighting

Manuscript received: September, 15, 2023; Revised December, 12, 2023; Accepted January, 16, 2024.

This paper was recommended for publication by Editor J. Borràs upon evaluation of the Associate Editor and Reviewers' comments. This work was supported by the Federal Ministry of Education and Research of the Federal Republic of Germany (BMBF) by funding the project ALD under Project no. 16ME0539K, and partially funded by the Lighthouse Initiative Geriatrics by StMWi Bayern (Project X, grant no. IUK-1807-0007// IUK582/001).

¹The authors are with the Munich Institute of Robotics and Machine Intelligence (MIRMI), Technische Universität München (TUM), Germany. {junnan.li, amartya.ganguly, haddadin}@tum.de

²L.F.C. Figueredo is with the School of Computer Science, University of Nottingham, UK. He is also an Associated Fellow at the MIRMI - TUM. figueredo@ieee.org

Digital Object Identifier (DOI): see top of this page.

[6], which presents an overview of wrench-based metrics for torque-actuated systems underscoring the performance mismatch from different conditions and assumptions to real-world experimental results. Similarly, the work [7] aimed to bridge the gap between conventional grasp-wrench metrics and the practice, exploring the capability of passively preserving the grasping equilibrium under the external wrench without changing actively commanded joint torques. The studies by [8], [12] extend the adoption of potential contact/grasp robustness metrics proposed in [9] for fully actuated hands to underactuated hands and utilize them to optimize design parameters for specific grasping tasks. The contributions of [10], [11] played a crucial role in expanding grasp wrench metrics to tendon-driven systems. They emphasized the asymmetric nature of manipulation tasks concerning contact forces on tendon-driven fingers, challenging the prevalent assumption of symmetry in conventional grasping metrics.

Existing experimental evaluation methods, such as the Anthropomorphic Hand Assessment Protocol, provide a replicable experimental protocol quantifying the ability of dexterous hands via a set of object manipulation tasks [13]. Therein, fifty dexterous taxonomies were selected as benchmark tests to evaluate static grasping as well as dynamic manipulation capabilities of a robotic hand [14]. The study demonstrates that degree of freedom (DOF) distribution and independence are key factors that would influence artificial hand dexterity. Overall, while empirical approaches are capable of revealing realistic performance compared to other methods (e.g., only quantitative algebraic metrics), the complexity of implementation and lengthy time cost reduce their application in iterative design optimization and task generalization.

In contrast, quantitative assessments benefit motion planning [15], [16] as well as design optimization [12], [17]. For example, Vahrenkamp et al. [18]–[20] extended the arm manipulability analysis through the workspace offering a comprehensive global evaluation supporting online robot base placement, grasping pose selection, and inverse kinematic (IK) solutions. A similar analysis was presented in our prior work in terms of human force generation capability with ergonomic considerations during human-robot interaction [21]. More specifically to finger design, You et al. [22] utilized the interactivity of finger metric to optimize the structure of a multi-fingered hand, yet focusing only on its kinematics.

While experimental evaluation approaches are costly and often task-specific, algebraic-based quantitative metrics focus on torque-actuated systems – evaluating the grasp quality with respect to the singular values of the grasping and Jacobian matrices – being unsuitable for systems with unilateral constraints, e.g., tendon forces, and object wrenches ignoring

the maneuverability of the system. More importantly, all these methods, and even the scarce results for tendon-driven systems, e.g., [10], [11], rely extensively on precise information regarding contact points and object properties. Consequently, they perform poorly when applied to hand or finger configurations that differ from the ones used in the original experiments or tasks. This limitation can result in higher planning costs when utilizing local online search techniques to find hand configurations, which may only be optimal within a limited context but sub-optimal in a broader perspective.

Our approach diverges from the majority of existing literature, aiming to assess the complete feasible workspace of both individual as well as multi-fingered systems. We propose three indexes quantifying individual task-independent capabilities of fingers that impact object stability and manipulability while satisfying unilateral tendon-driven force constraints. Then, we introduce a generalized metric by combining these indexes to provide a comprehensive evaluation of the performance of tendon-driven robotic hands. We further evaluate by demonstrating the simulated Shadow Hand as an example and illustrating a practical application of optimizing the pre-grasping pose by leveraging the evaluation results.

II. MATHEMATICAL BACKGROUND

Consider a tendon-driven robotic finger with m joints and n tendons. The n -dimensional tendon forces (\mathbf{f}_{td}) are conveyed through a tendon routing configuration to yield m -dimensional joint torques ($\boldsymbol{\tau}$). The finger interacting with an object yields fingertip forces (\mathbf{f}_{ft}) at joint configuration \mathbf{q} .

The dynamics of the robotic finger is formulated as

$$\mathbf{M}(\mathbf{q})\ddot{\mathbf{q}} + \mathbf{N}(\mathbf{q}, \dot{\mathbf{q}}) + \mathbf{G}(\mathbf{q}) + \mathbf{J}(\mathbf{q})^T \mathbf{f}_{ft} = \boldsymbol{\tau}, \quad (1)$$

$$\boldsymbol{\tau} = \mathbf{C} \mathbf{f}_{td}; \quad (2)$$

$$\mathbf{f}_{td(i)} \in [\mathbf{f}_{td(i, \min)}, \mathbf{f}_{td(i, \max)}] \text{ with } i = 1, 2, \dots, n; \quad (3)$$

$$\boldsymbol{\Omega} = \mathbf{H} \mathbf{f}_{ft}, \quad (4)$$

where, $\mathbf{f}_{td} = [\mathbf{f}_{td(1)}, \dots, \mathbf{f}_{td(n)}]^T \in \mathbb{R}^n$ and $\boldsymbol{\tau} \in \mathbb{R}^m$ represent force vector of n tendons and generalized joint torque, respectively. $\mathbf{M}(\mathbf{q}) \in \mathbb{R}^{m \times m}$ is the positive definite inertia matrix. $\mathbf{N}(\mathbf{q}, \dot{\mathbf{q}}) \in \mathbb{R}^m$ is the centripetal and Coriolis forces and $\mathbf{G}(\mathbf{q}) \in \mathbb{R}^m$ is the generalized gravity force. $\mathbf{f}_{ft} \in \mathbb{R}^3$ consists of the fingertip translational forces interacting with objects and $\mathbf{J}(\mathbf{q})^T \in \mathbb{R}^{m \times k}$ is the transpose of Jacobian matrix at a point on the fingertip. The tendon routing configuration of the robotic finger is represented by a coupling matrix $\mathbf{C} \in \mathbb{R}^{m \times n}$ which defines the mapping of the tendon forces to that of the joint torque. Each element $c_{i,j} \in \mathbf{C}$ with $i = \{1, \dots, m\}$ $j = \{1, \dots, n\}$ represents the moment arm of tendon j to joint i , with $c_{i,j} > 0$ representing flexors, whereas, $c_{i,j} < 0$ represents extensors. The grasping matrix \mathbf{H} conveys the contact forces \mathbf{f}_{ft} to the object wrench $\boldsymbol{\Omega}$.

As the potential interactions lie in the operational space, the dynamics of the finger without contact can be expressed in the operational space proposed in [23] as

$$\mathbf{A}(\mathbf{x})\ddot{\mathbf{x}} + \tilde{\mathbf{N}}(\mathbf{x}, \dot{\mathbf{x}}) + \tilde{\mathbf{G}}(\mathbf{x}) = \mathbf{J}^{+T} \boldsymbol{\tau}, \quad (5)$$

where, $\mathbf{A}(\mathbf{x})$ is the operational inertia matrix derived from

$$\mathbf{A}(\mathbf{x}) = \mathbf{J}^{+T}(\mathbf{q})\mathbf{M}(\mathbf{q})\mathbf{J}^+(\mathbf{q}). \quad (6)$$

$\tilde{\mathbf{N}}, \tilde{\mathbf{G}}$ are the centripetal, and Coriolis, and gravity forces in operational space, while \mathbf{J}^+ denotes the pseudo-inverse \mathbf{J} .

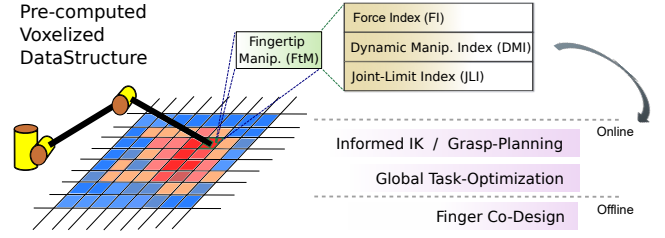


Fig. 1: Illustration of the assessment data structure. The fingertip space is voxelized (one 2D sliced plane). FI, DMI, and JLI are calculated for each voxel and integrated into FtM assessment. These data enable versatile applications in both online and offline scenarios.

III. FINGERTIP MANIPULABILITY ASSESSMENT

We are computing and analyzing a quality index for different tasks in different configurations of the workspace of a tendon-driven multi-fingered system.

To this aim, we propose an augmented $\mathbb{R}^3 \times \mathcal{S}^3 \times \mathcal{S}$ voxelized data structure that incorporates, in each voxel, features related to the object stability and constrained dynamic manipulability.¹ These features are better depicted in Fig. 1. The Force Index (FI) metric captures the object stability in terms of the maximum fingertip force (\mathbf{f}_{ft}) capability in multiple directions. More specifically, it unfolds the average fingertip force resistance, which can be thereafter used for force-closure analysis. The FI is detailed in Subsection III-B.

The Dynamic Manipulability Index (DMI) quantifies the task-space achievable acceleration in all directions. It effectively describes the maneuverability of the finger within the workspace, with variations that become particularly evident in scenarios like singularities. This metric is further detailed in Subsection III-C.

Finally, the Joint Limits Index (JLI) captures the distance to the \mathbb{R}^m subspace of valid configurations given the finger design. The computation of JLI is given in Subsection III-D.

The voxelized data structure reveals distinct aspects of the finger's capability across the workspace. In most cases, individual features are achieved in exchange for others, e.g., force capabilities in singularities. For a more comprehensive assessment, we also propose Fingertip Manipulability (FtM); a composite metric incorporating both object stability and manipulability. The metric can be quickly adapted to different task goals. This allows for comprehensive or task-informed-IK solutions for finger and wrist placement, and an overview of the interaction workspace of multi-fingered systems.

The following assumptions have been made to clarify the scope of this paper.

- Fingertip force closure with frictional point contact, indicates that the finger interacts with the objects solely at the fingertip and only translational forces can be conveyed at the point of contact on the object;
- A redundant tendon-driven system, indicating the surjective map from tendon forces via joint torques to the fingertip forces;²

¹The discretization of the workspace follows a similar procedure to [21].

²The dimensions of variables in (1) (2) (4) follow $n \geq m \geq k = 3$

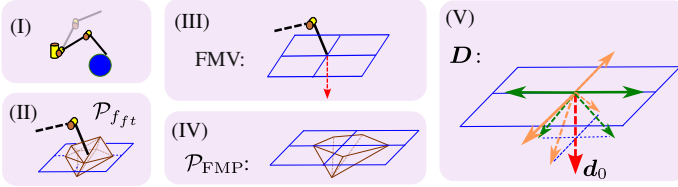


Fig. 2: Illustrates the process of calculating FI. At this configuration in (I), the translational fingertip force polytope $\mathcal{P}_{f_{ft}}$ is shown in brown in (II). The FMV vector is depicted in (III) in red. (IV) shows the \mathcal{P}_{FMP} truncated by the plane (blue) defined by FMV. One example of the discretization method for computing FI with nine vectors ($r = 9$) is shown in (V), where the vectors in the same plane are encoded in the same color, and the FMV is illustrated in red.

- Low mass property³ (negligible gravity) and quasi-static condition (velocity-related term $\mathbf{N}(\mathbf{q}, \dot{\mathbf{q}})$ is zero).

A. Feasible Polytopes

In robotics, force and motion generation capabilities are often connected to manipulability metrics and the manipulability ellipsoid [24]. The manipulability ellipsoid conveys a local picture of the operational space (for example, contact force \mathbf{f}) capabilities given the local deformation/transformation of a unit norm of joint-space torques, that is,

$$\boldsymbol{\tau}^T \boldsymbol{\tau} = \mathbf{f}^T \mathbf{J}(\mathbf{q}) \mathbf{J}^T(\mathbf{q}) \mathbf{f}, \quad (7)$$

where $\|\boldsymbol{\tau}\|_2$ relies on the L_2 -norm of a vector space, e.g., joint torques. In the case of tendon-driven system (1)-(4), where actuation based on tendon forces follow unilateral constraints (i.e., a tendon can only be pulled), such transformation is not realistic or achievable, as previously shown in [21]. Alternatively, the polytope representation, which satisfies the L_∞ -norm boundary conditions (maximal and minimal tendon forces), is employed to depict the feasible region of target space $\mathcal{P}_\mathcal{X}$ (such as fingertip force) from the tendon force space \mathcal{X} formulated as

$$\mathcal{P}_\mathcal{X} = \{\mathbf{x} \in \mathcal{X} \subseteq \mathbb{R}^n : \mathbf{A}_\mathcal{X} \mathbf{x} \leq \mathbf{b}_\mathcal{X} \cap \mathbf{C}_\mathcal{X} \mathbf{x} = \mathbf{d}_\mathcal{X}\}, \quad (8)$$

where $\mathbf{A}_\mathcal{X} \in \mathbb{R}^{m_i \times n}$, $\mathbf{C}_\mathcal{X} \in \mathbb{R}^{m_e \times n}$, $\mathbf{b}_\mathcal{X} \in \mathbb{R}^{m_i}$, and $\mathbf{d}_\mathcal{X} \in \mathbb{R}^{m_e}$, depicts a set of constraints of \mathbf{x} in an n -dimensional physical projected space \mathcal{X} . The polytope provides a more accurate representation of the boundaries in the target space than the ellipsoid representation [25].

B. Force Index

We introduce the Force Index (FI), a metric designed to assess the ability of the finger to generate contact force to maintain the stability of an object when subjected to wrench disturbance. This ability is quantitatively expressed by calculating the weighted mean of the peak fingertip forces, considering the various directions in which the finger can apply force to objects. The constraints imposed by tendon force in a specific routing configuration determine the direction of the forces applied by the finger

With the given configuration \mathbf{q} , Fig. 2(I), the feasible fingertip force is derived from the tendon force limits and represented as the polytope $\mathcal{P}_{f_{ft}}(\mathbf{q})$, illustrated as Fig. 2(II).

³The gravity can also be considered in the metric computation while computing the joint torque polytope.

To compute the polytope $\mathcal{P}_{f_{ft}}(\mathbf{q})$, we first define the augmented variable

$$\mathbf{x} = [\mathbf{f}_{td}^T \quad \boldsymbol{\tau}^T]^T. \quad (9)$$

The convex polytope constrained by the tendon force limits in (2)-(3) is expressed as

$$\mathcal{P}_\mathcal{X} = \{\mathbf{x} \in \mathbb{R}^{n+m} : \mathbf{A}_\mathcal{X} \mathbf{x} \leq \mathbf{b}_\mathcal{X} \cap \mathbf{C}_\mathcal{X} \mathbf{x} = \mathbf{d}_\mathcal{X}\}, \quad (10)$$

$$\mathbf{A}_\mathcal{X} = \begin{bmatrix} \mathbf{I} & \mathbf{0} \\ -\mathbf{I} & \mathbf{0} \end{bmatrix}; \quad \mathbf{b}_\mathcal{X} = \begin{bmatrix} \mathbf{f}_{t,\max} \\ -\mathbf{f}_{t,\min} \end{bmatrix}, \quad (11)$$

$$\mathbf{C}_\mathcal{X} = [\mathbf{C}(\mathbf{q}) \quad -\mathbf{I}]; \quad \mathbf{d}_\mathcal{X} = [0 \quad 0 \quad 0]^T, \quad (12)$$

where, \mathbf{I} and $\mathbf{0}$ are the identity and zero matrices. Truncating the constraints (11)-(12) relates to the tendon forces and joint torques from (2)-(3). From the polytope of the augmented variable \mathbf{x} , the n -dimensional feasible torque polytope \mathcal{P}_τ and 3D translational fingertip force polytope $\mathcal{P}_{f_{ft}}(\mathbf{q})$ can be extracted by truncating the convex polytope $\mathcal{P}_\mathcal{X}$

$$\mathcal{P}_\tau(\mathbf{q}) = [0 \quad \mathbf{I}] \mathcal{P}_\mathcal{X}, \quad (13)$$

$$\mathcal{P}_{f_{ft}}(\mathbf{q}) = \mathbf{J}^{+T}(\mathbf{q}) \mathcal{P}_\tau(\mathbf{q}), \quad (14)$$

Due to the unilateral constraint of frictional contact, only the fingertip force orienting to the object half-space can be conveyed to the object. We, therefore, truncate the polytope $\mathcal{P}_{f_{ft}}(\mathbf{q})$ with a plane through the fingertip point as shown in blue in Fig. 2(II). The fingertip-applied forces are, therefore, defined along a half-plane.

To easily adapt the half-plane to task-specific information, if available, we introduce the Force-Manipulating Vector (FMV) $\mathbf{d}_0 \in \mathbb{R}^3$, illustrated in red in Fig. 2(III). The FMV indicates the expected force direction to be exerted at the object and provides the designer with an easy tool to define the half-space for the truncated fingertip force polytope, Fig. 2. For task-independent evaluation, FMV can be broadly defined as a vector oriented to the center of the object workspace, where the object is expected to be located with potential for mobility in each direction. Conversely, for task-specific evaluation with well-defined information, such as grasping pose and contacts, FMV can be tailored as the normal contact force vector for each fingertip, focusing on the interaction forces at the designated grasping pose.

The truncated polytope, denoted as $\mathcal{P}_{FMP}(\mathbf{q})$ and visualized in brown in Fig. 2(IV), is formulated as

$$\mathcal{P}_{FMP}(\mathbf{q}) = \{\mathbf{x} \in \mathcal{P}_{f_{ft}}(\mathbf{q}) : -\mathbf{d}_0^T \mathbf{x} < 0\}, \quad (15)$$

where, the inequality ensures the resulting polytope stays in the same half-space represented by FMV (\mathbf{d}_0).

The mean peak force of \mathcal{P}_{FMP} , termed as $\tilde{\mathcal{J}}_f(\mathbf{q})$, is calculated by integrating the distance of all the points on the surface of polytope (each point represents the maximum force in the relevant direction)

$$\tilde{\mathcal{J}}_f(\mathbf{q}) = \frac{1}{\text{Area}(S)} \iint_S \|\mathbf{x}\| d\sigma; \quad \mathbf{x} \in \mathcal{P}_{FMP}, \quad (16)$$

where, S represents the surfaces of $\mathcal{P}_{FMP}(\mathbf{q})$. $\|\mathbf{x}\|$ is the distance from the origin to each point σ on the surface, indicating the peak force along the direction of \mathbf{x} . However, the calculation of $\tilde{\mathcal{J}}_f(\mathbf{q})$ is computationally expensive due to the complex constraints of the polytope. To minimize computational effort, we employ an alternative method to approximate the $\tilde{\mathcal{J}}_f(\mathbf{q})$. We first introduce r directional vectors,

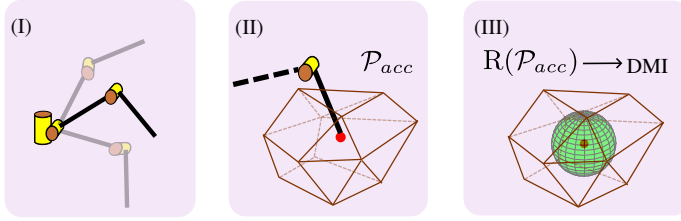


Fig. 3: Consider a single configuration \mathbf{q} within the workspace, as seen in (I). We can visualize the fingertip acceleration polytope, denoted as \mathcal{P}_{acc} , shown in brown in panel (II). In panel(III), we observe the largest sphere, highlighted in green, which is inscribed within \mathcal{P}_{acc} and centered at the fingertip depicted in red. The radius of this inscribed sphere, denoted as $R(\mathcal{P}_{acc})$, served as parameter for calculating DMI.

denoted as $\mathbf{D} = [\mathbf{d}_0, \dots, \mathbf{d}_{r-1}] \in \mathbb{R}^{r \times 3}$, to discretize the half-space (\mathbf{d}_0 refers to FMV). Then, we introduce FI denoted as $\mathcal{J}_f(\mathbf{q})$, which is the mean of the peak forces along all r directions weighted by \mathbf{w} , to represent the $\tilde{\mathcal{J}}_f(\mathbf{q})$ as

$$\mathcal{J}_f(\mathbf{q}) = \frac{1}{\|\mathbf{w}\|} \sum_{i=0}^{r-1} w_i \max(z), \text{ s.t. } z\mathbf{d}_i \in \mathcal{P}_{FMP}(\mathbf{q}), \quad (17)$$

where, $\mathbf{w} \in \mathbb{R}^r$ is the pre-defined weight vector for each directions. z is a scalar and $\max(z)$ refers to the peak f_{ft} along each direction of \mathbf{d}_i . It is crucial to emphasize that within the weight vector \mathbf{w} , some elements have the flexibility to be set to zero, indicating directions that are inconsequential. This adaptability enables FI to be customized for particular tasks, focusing on the key directions of the fingertip force.

As an example, in Fig. 2(V), we have discretized the space using a grid with a resolution of $r = 9$. In this configuration, there are four vectors highlighted in orange that are positioned in the Y-Z plane. These vectors divide the half-plane into four equal sections, each spanning 45° . This arrangement is mirrored by another set of four vectors shown in green, which lie in the X-Z plane and serve the same purpose as the orange vectors. Then, the intersection points of all vectors with the $\mathcal{P}_{FMP}(\mathbf{q})$ are marked in red, indicating the peak fingertip forces, as shown in Fig. 2(IV).

C. Dynamic Manipulability Index

Dynamic Manipulability Index (DMI) is a metric that quantifies the maximum translational Cartesian acceleration achievable by the fingertip in all directions, with respect to specific configuration \mathbf{q} and tendon force limits. This is similar to the acceleration radius metric proposed in [26] but adapted to function as a localized metric at \mathbf{q} . In other words, DMI provides a quantitative representation of the ability of a finger to perform precise and skillful manipulations.

Assuming no external contact with the finger, Fig. 3(I), the translational acceleration of the fingertip $\ddot{\mathbf{x}}$ defined in (5) can be expressed as a function of the joint torque from (5)-(6)

$$\ddot{\mathbf{x}} = \mathbf{J}(\mathbf{q})\mathbf{M}^{-1}(\mathbf{q})\boldsymbol{\tau}. \quad (18)$$

The feasible acceleration polytope of the fingertip constrained by the tendon force limits can be derived from the joint torque polytope \mathcal{P}_τ in (13)

$$\mathcal{P}_{acc} = \mathbf{J}(\mathbf{q})\mathbf{M}^{-1}(\mathbf{q})\mathcal{P}_\tau. \quad (19)$$

which is illustrated in Fig. 3(II).

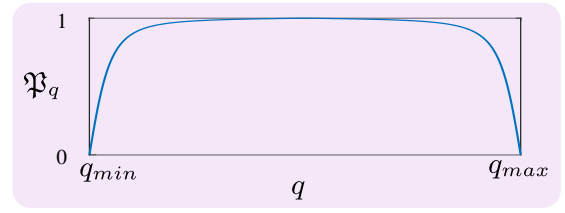


Fig. 4: An illustration the JLI curve for one joint. The value achieves maximum $\mathfrak{P}_q = 1$, when $q = (q_{min} + q_{max})/2$, while decreasing to 0 towards joint limits.

The DMI $\hat{\mathfrak{P}}_{acc}$ at joint configuration \mathbf{q} is formulated as

$$\hat{\mathfrak{P}}_{acc}(\mathbf{q}) = \frac{R(\mathcal{P}_{acc}(\mathbf{q}))}{R_{max}} \quad (20)$$

where $\hat{\cdot}$ donates the normalized term. $R(\mathcal{P}_{acc}(\mathbf{q}))$ is the radius of the largest sphere centered at the origin inscribed in the acceleration polytope \mathcal{P}_{acc} at configuration \mathbf{q} , Fig. 3(III). R_{max} refers to the maximum radius for all the sample configurations spanning the entire voxelized fingertip workspace.

D. Joint Limits Index

We utilize the Joint Limits Index (JLI) function proposed in [18]. Denoting the upper and lower limits of the i^{th} joint as $q_{i,min}$ and $q_{i,max}$, the penalty term $\mathfrak{P}_{q,i}(q)$ of the joint i^{th} at joint configuration q_i is formulated as

$$\mathfrak{P}_{q,i}(q_i) = \frac{1}{\sqrt{1 + |\nabla h(q_i)|}}; \quad (21)$$

where, $\nabla h(q_i)$ is the gradient of the joint potential defined as

$$\nabla h(q_i) = \frac{(q_{i,max} - q_{i,min})^2(2q_i - q_{i,max} - q_{i,min})}{4(q_{i,max} - q_i)^2(q_{i,min} - q_i)^2}. \quad (22)$$

An example of the $\mathfrak{P}_q(q)$ curve for one joint is shown in Fig. 4. It affects joint configurations close to their limits, restricting finger movement when approaching extremes. This addresses and discourages potentially unsafe or unrealistic joint positions.

For a finger with m joints, JLI $\hat{\mathfrak{P}}_q(\mathbf{q})$ is defined as

$$\hat{\mathfrak{P}}_q(\mathbf{q}) = \prod_{i=1}^m \mathfrak{P}_{q,i}(q), \quad (23)$$

where, $\hat{\mathfrak{P}}_q(\mathbf{q}) \in (0, 1]$.

E. Fingertip Manipulability

For a comprehensive evaluation that incorporates both fingertip force and manipulability, we propose the metric termed Fingertip Manipulability (FtM) denoted as \mathfrak{M} as a way to integrate all three terms at the joint configuration \mathbf{q} :

$$\mathfrak{M}(\mathbf{q}) = \hat{\mathfrak{P}}_q(\mathbf{q})\hat{\mathfrak{P}}_{acc}(\mathbf{q})\mathcal{J}_f(\mathbf{q}) \quad (24)$$

where, $\hat{\mathfrak{P}}_{acc}(\mathbf{q})$ and $\hat{\mathfrak{P}}_q$ vary from zero to one across the configurations, acting as penalty terms on FI. As a composite metric, FtM represents the weighted average of peak force produced by the fingertip, adjusted for the fingertip's ability to reposition itself. Notably, the method of combining these elements is not fixed and can be customized to suit specific tasks. FtM is a general evaluation metric of fingertip force and manipulability while grasping an object. To establish a global data structure for storing evaluation information, FtM, we voxelized the fingertip workspace. Alternatively, a workspace

discretization of the joint-space is also possible but lacks operational space information.

Since the metrics are the functions of joint configurations, we discretize the \mathbb{R}^3 fingertip space into voxels and compute the IK for each voxel to fit the metric input. In the context of a redundant system, the mapping from joint configuration to fingertip position is not unique. Selecting the optimal pose from among the nullspace solutions is computationally intensive, particularly for real-time applications. However, by storing the pose associated with the most favourable assessment for each voxel, we reduce the computational burden of online nullspace IK calculation and grasp planning. Consequently, to compute the optimal nullspace pose, we generate a random set of nullspace IK solutions for each voxel $\mathbf{x}_i \in \mathbb{R}^3$ within the fingertip space. The configuration that yields the greatest FtM value is designated as the optimal grasp pose for this voxel. Subsequently, we store not only its IK solution but also metrics such as FI, DMI, JLI, and FtM information within our data structure. By processing all the voxels, we obtain a comprehensive global representation within our data structure, effectively capturing essential evaluation data in an efficient manner.

IV. RESULTS OF FTM ASSESSMENT

1) *Evaluation of a single Finger*: Using the index finger of a Shadow Hand [27] as an example, we illustrate the distribution of FtM and the associated metrics, FI, DMI and JLI. The kinematic and dynamic parameters necessary for the analysis are extracted from the Shadow Hand specification [27]. The kinematic model of the Shadow Hand is illustrated in Fig. 5(I). Due to the unavailability of tendon routing information, we make the assumption that the finger is driven by 8 individual tendons with constant moment arms following a 2N structure. This assumption allows us to define the coupling matrix C_4 of the index finger with 4 DoF

$$C_4 = \begin{bmatrix} 1 & -1 & 1 & -1 & 1 & -1 & 1 & -1 \\ 1 & 1 & 1 & 0 & -1 & -1 & -1 & 0 \\ 1 & 1 & 0 & 0 & -1 & -1 & 0 & 0 \\ 1 & 0 & 0 & 0 & -1 & 0 & 0 & 0 \end{bmatrix} \quad (25)$$

The coupling matrix is designed isometrically with an equal number of extensors and flexors for each joint. Each tendon is actuated individually by a motor, assuming to provide the tendon force from a minimum of 0.5 N to a maximum of 100 N. The initial pose with $\mathbf{q} = \mathbf{0}$ of the index finger is defined within the X-Z plane forming a 30° angle with respect to the X-axis. The FMV \mathbf{d}_0 , \mathbf{D} , and the weight vector \mathbf{w} are defined as

$$\mathbf{d}_0 = [0, 0, -1]^T; \quad (26)$$

$$\mathbf{D} = \begin{bmatrix} 0 & a & -a & 0 & 0 & 1 & -1 & 0 & 0 \\ 0 & 0 & 0 & a & -a & 0 & 0 & 1 & -1 \\ -1 & -a & -a & -a & -a & 0 & 0 & 0 & 0 \end{bmatrix}, \quad a = \frac{\sqrt{2}}{2}; \quad (27)$$

$$\mathbf{w} = [2, 1, 1, 1, 1, 1, 1, 1]. \quad (28)$$

The FMV is set oriented to the negative Z-axis, indicating objects are manipulated underneath the index fingertip. In this example, \mathbf{D} is defined as in Fig. 2 to compute FI. The weight vector \mathbf{w} ensures all direction vectors are considered, with the direction \mathbf{d}_0 given double weight in our assessment.

For each voxel, nullspace IK solutions are randomly calculated. The distribution of the FI values is visualized in Fig. 5(II). The FI values across the voxelized space have global values between 38.17 and 89.32. The example configuration, fingertip highlighted by a green point, achieves a FI value of 43.96, indicating the weighted peak \mathbf{f}_{ft} along nine directions. The slice of voxels situated near the maximum point along the X-axis in the green-circled area achieves a range from 68 to 82. These configurations display greater FI values because of high force resistance along the singular direction $\mathbf{d}_5 = [1, 0, 0]^T$. However, these configurations have limited capability to manipulate the the fingertip along \mathbf{d}_5 due to the small singular value of the Jacobian matrix. This constraint is not evident from the FI assessment alone.

To address these cases, we incorporate the DMI into the assessment by multiplying FI and DMI terms. The DMI reveals the capability of accelerating the fingertip in all directions as depicted in Fig. 5(III). Since the DMI is normalized, the value indicates the ratio of the maximal omnidirectional acceleration achievable by this configuration to the maximum DMI value of all voxels. The result of the FI-DMI assessment is illustrated in Fig. 5(IV), where the configurations close to the singularity are now penalized due to the limited manipulability.

Another limitation emerges from configurations near joint-space boundaries ignoring the fact that the finger should be physically constrained to those. This is better visualized in indexes close to workspace boundaries. To address this issue, we introduce JLI, which is visualized in Fig. 5(V). The example configuration achieves a JLI value of 0.96 indicating the finger's capability in this configuration is barely affected by the joint limits. The FtM assessment is synthesized by integrating the JLI, as seen in Fig. 5(VI). The JLI penalizes the assessment of configurations close to limits. The example configuration achieves a value of 10.55 within a global range from 0 to 62.67 for FtM assessment given tendon force limits.

2) *Evaluation of a Multi-fingered Hand*: Extending FtM assessment to all fingers, the global representation of the multi-fingered hand is illustrated by taking the Shadow Hand as an example, Fig. 6. The thumb and little finger of the Shadow Hand have 5 Dof, while the index, middle, and ring fingers have identical configurations of 4 Dof. For the sake of simplification, the FtM representation of the index finger from Fig. 5(VI) is taken to represent both the middle and ring finger. We make the identical assumption of tendon force limits within a range of 0.5 to 100 N. The coupling matrix C_5 for both 5-DoF thumb and little finger is defined as

$$C_5 = \begin{bmatrix} 1 & -1 & 1 & -1 & 1 & 1 & -1 & 1 & -1 & 1 \\ 1 & 1 & 1 & 1 & 0 & -1 & -1 & -1 & -1 & 0 \\ -1 & 1 & -1 & 0 & 0 & -1 & 1 & -1 & 0 & 0 \\ 1 & 1 & 0 & 0 & 0 & -1 & -1 & 0 & 0 & 0 \\ 1 & 0 & 0 & 0 & 0 & -1 & 0 & 0 & 0 & 0 \end{bmatrix}, \quad (29)$$

Based on the kinematic configuration of the Shadow Hand, the FMV and weight vectors \mathbf{w} of each finger are defined as

$$\mathbf{d}_{0,index} = [0, 0, -1]^T; \quad \mathbf{d}_{0,thumb} = \left[0, -\frac{\sqrt{2}}{2}, \frac{\sqrt{2}}{2}\right]^T; \quad (30)$$

$$\mathbf{d}_{0,little} = -\mathbf{d}_{0,thumb}; \quad \mathbf{w} = [2, 1, 1, 1, 1, 1, 1, 1, 1]. \quad (31)$$

The FMV of the thumb and little finger are defined based on the position of fingertips to the center of all fingertips while forming general caging grasps without defining objects. The

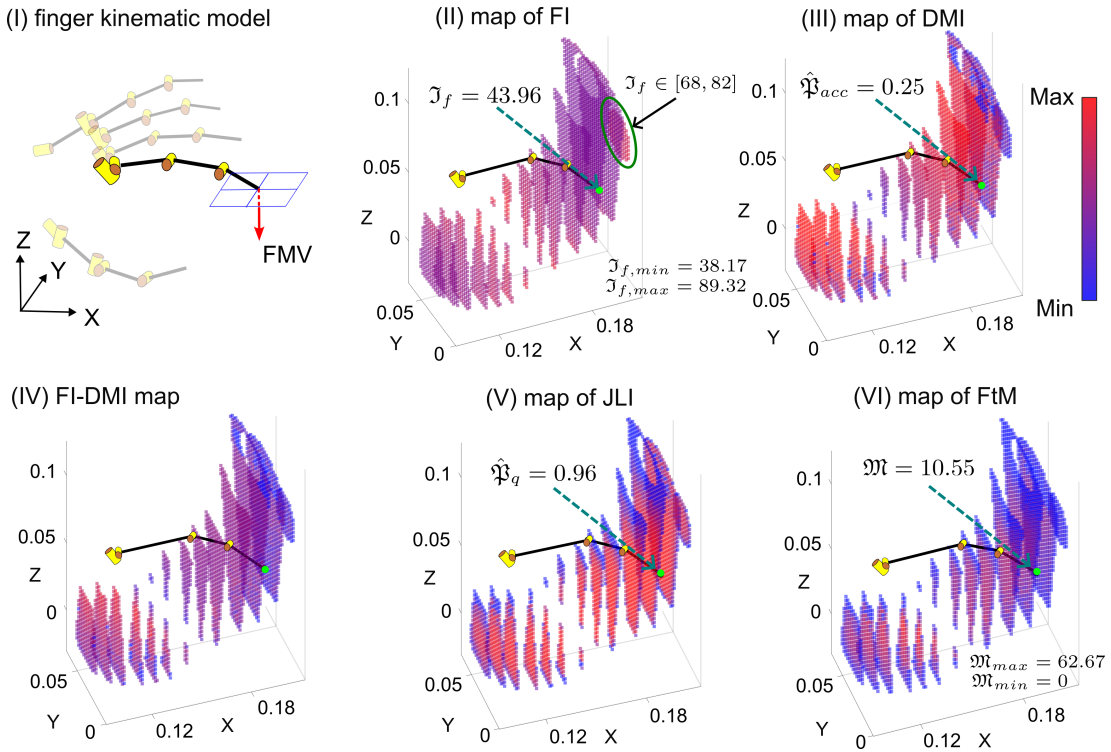


Fig. 5: (I) illustrates the kinematic model of the shadow hand with the index finger and pre-defined FMV vector highlighted. (II) shows the sliced distribution of the FI values (\mathcal{J}_f) of the index finger throughout the voxelized workspace of the fingertip. The fingertip point of the example pose is highlighted in green, and the FI value of that configuration is depicted. (III) visualized the sliced colored map of the DMI values ($\hat{\mathfrak{P}}_{acc}$). In (IV), it shows the sliced map of FI penalized by the DMI, where the singularity along the directions, for instance, along positive X-axis, is penalized. (V) depicts the sliced distribution of the JLI values, and the FtM index is visualized in (VI).

matrix D for the thumb and little finger undergo the same rotation as $d_{0,thumb}$ and $d_{0,little}$ to align with $d_{0,index}$. The global FtM representation of the thumb, index, and little finger are visualized in Fig. 6(I)(II)(IV) separately for the sake of a clear visualization.

The global representation stores the FtM information of all fingers within each fingertip space, sharing the same Cartesian space. Consequently, it provides the assessment information of each fingertip when the grasping pose is specified. The global assessment can serve as an objective by integrating the FtM assessment of all fingertips that facilitates direct comparison of grasping capabilities among different grasping poses and to identify the optimal object placement and grasping pose for a specific task, as illustrated upon in Sec. V.

V. APPLICATION

In this section, for brevity, we focus on one example scenario of multi-fingered grasping and propose the algorithm of applying the global FtM assessment as objective to optimize the object placement and grasping pose.

Scenario description: Grasping an object with a multi-fingered hand with fingertips. The position and orientation of the object center relative to the hand base are denoted as $s_o = [x_o^T, \phi_o^T]^T \in \mathbb{R}^6$. The object has n_c pre-defined potential contact points fixed in the object frame whose indices comprise the set $S = \{1, \dots, n_c\}$. Therefore, the Cartesian position of all contact points is a vector associated with the object pose s_o denoted as $x(s_o) = [x_1(s_o), \dots, x_{n_c}(s_o)]$. The

multi-fingered hand has n_f fingertips whose indices comprise the set $F = \{1, \dots, n_f\}$ with $n_f \leq n_c$. Each fingertip in set F interacts with the object at one contact point defined in the set S . Mathematically speaking, an injective mapping f describes the relationship of fingertip index set F to the contact point index set S formulated as $f: F \rightarrow S$.

Problem definition: Given the position information of all pre-defined contacts, i.e. $x(s_o)$, find the object placement (s_o) and grasping pose (f) such that the objective cost is maximized. Here, as an example, the cost is designed as the multiplication of the normalized FtM of all fingertips in order to mitigate the bias of fingertip forces caused by different numbers of tendons among fingers. As scaling the cost with a constant value (maximal FtM value of each fingertip) does not influence the results, the normalized FtM is replaced as the FtM value in the implementation and formulated as

$$p = \max_{s_o, f} \prod_{\forall i \in F} \mathfrak{M}_i(x_{f(i)}(s_o)); \quad (32)$$

$$\text{s.t. } \forall i \in F: d_{0i}^T \cdot (x_o - x_{f(i)}(s_o)) > 0; \quad (33)$$

where, d_{0i} denotes the FMV of the i^{th} fingertip. The constraint in (33) ensures that all the contact satisfies the unilateral constraint, i.e., all the interaction forces exerted by fingertips orient into the object.

As an example to show pre-grasping pose optimization algorithm based on the global FtM information, we define a sphere with a radius of $r = 25\text{mm}$ to be grasped by three fingers, which are the thumb, index, and middle fingers of the

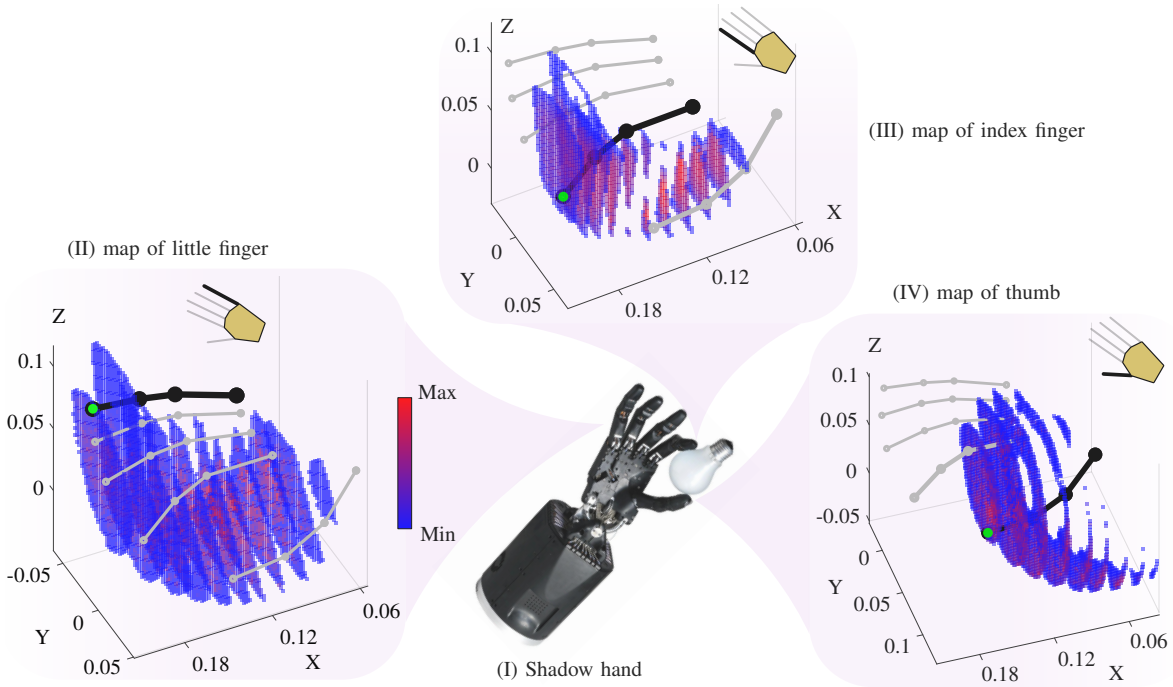


Fig. 6: Results of the FtM evaluation for the shadow hand. The shadow hand is shown in (III) with an example pose of grasping. The colored assessment maps of the index, little finger, and thumb are illustrated in (II), (I), and (IV), respectively. In each map, the hand remains the same grasping pose, and the corresponding finger is highlighted in black with its fingertip point in green.

shadow hand, via three pre-defined contact points illustrated in Fig. 7(I). In this case, the number of contact points is equal to that of fingers, thus, the mapping f is bijective. The FtM map of these three fingers is visualized as Fig. 7(II) in the Cartesian space. Using the Particle Swarm Optimization algorithms and customized toolbox in MATLAB, the sequential optimization results of the grasping pose of these three fingers are illustrated in Fig. 7(III) with the increasing objective value p .

VI. DISCUSSION AND CONCLUSIONS

In this work, we utilize metrics (FI, DMI, and JLI) to evaluate distinct finger capabilities in order to reveal the performance of the finger in object manipulation tasks with solely finger information. This leads to plausible evaluations that are adaptable to any specific task, as compared to the task-dependent metrics outlined in [5], which require the contact information given by specific tasks. Then, we design

a composite metric FtM formed by multiplying all the sub-metrics. This integration manner of multiplication makes FtM a comprehensive metric by taking all aspects captured by each individual metric into account.

It is critical to emphasize that the way of integrating metrics to form FtM is not unique, and the method depicted in this work is one universal way without task-specific focus. This flexibility allows for the customization of FtM to align with the specific requirements of each task. For instance, in a simple task where the finger is solely required to apply force predominantly in one direction, such as pressing a button. The presence of a singularity in the fingertip force along that particular direction can be advantageous because it enables a high force resistance in that direction. However, it is worth noting that the singularity of the Jacobian is often assessed as an unfavourable configuration in certain analyses, such as manipulability analysis [2][18]. In some

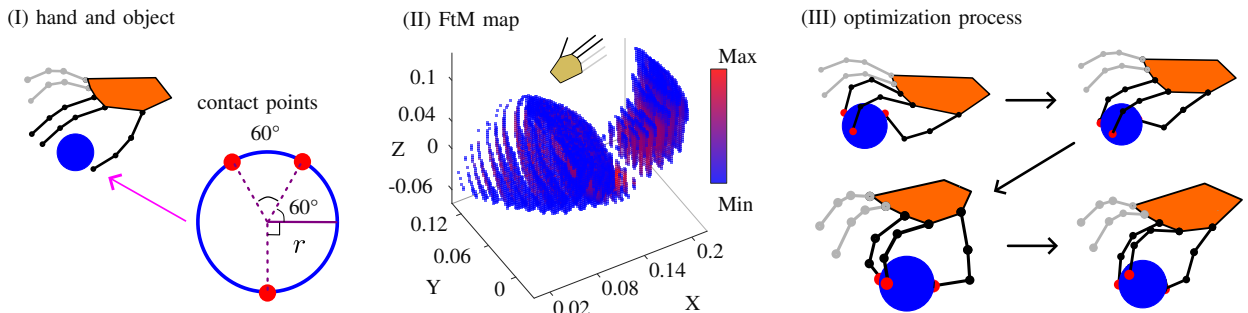


Fig. 7: (I) depicts the three-fingers model of the shadow hand and the pre-defined sphere with three contact points. (II) shows the colored map of the three-fingers hand. (III) shows the resulting poses during optimization with increasing objectives.

cases, closeness to singularity facilitates the task performance by gaining higher stiffness in the specific direction [25]. This can be addressed by appropriately tailoring the FtM metric, for example, undermining the DMI and JLI from the FtM assessment. Moreover, task-agnostic and task-specific evaluation can be achieved by defining FMV and weight vector accordingly. Aiming for the former and considering objects manipulated within the palm amid the fingertips of a multi-fingered hand, the FMV can align from the fingertip orienting to the center of the object workspace, where the object is expected to be located. Combined with a unitary weight vector, the FI metric takes the majority of in-hand manipulation and grasping scenarios into account. Conversely, for realizing task-specific evaluation in a well-defined grasping scenario, FMV can be customized as the normal vector of contacts to focus on the interaction forces crucial for the grasping performance. Task-independent evaluation is solely associated with finger-centric parameters, therefore, it substantially matches the multipurposed characteristic of the dexterous hand. In addition, the metrics can be utilized in the design phase even if the task for the hand is not defined.

As a unified global data structure, the FtM assessment assumes the role of an objective cost in the optimization process, such as pre-grasping planning. It could be defined within either configuration or fingertip spaces. However, given the contacts are normally constrained in the Cartesian space, it is computationally efficient to represent in the same space (i.e. fingertip space) to avoid the inverse kinematic computation.

The proposed evaluation can be adapted to the torque-driven robotic hand by directly defining the joint torque polytope according to the motor limits. However, these metrics have limitations as they are based on the assumption of rigid links, which makes it challenging to adapt to soft hands. The ignored factors, i.e. joint or tendon friction, may also cause the bias of the evaluation. Future work will encompass the analysis of underactuated systems – through augmented mapping to the multi-fingered cooperative-space under the tendon-force influence. Additionally, there are plans to extend applications to tasks such as optimizing the tendon routing system of the robotic finger using the FtM as a guiding metric, as well as the design of a benchmark platform for quantitative comparison between different metrics under torque-actuated and tendon-driven systems.

REFERENCES

- [1] V. Ortenzi, M. Controzzi, F. Cini, J. Leitner, M. Bianchi, M. A. Roa, and P. Corke, "Robotic manipulation and the role of the task in the metric of success," *Nature Machine Intelligence*, vol. 1, no. 8, pp. 340–346, 2019.
- [2] M. A. Roa and R. Suárez, "Grasp quality measures: Review and performance," *Autonomous robots*, vol. 38, no. 1, pp. 65–88, 2015.
- [3] T. Yoshikawa, "Manipulability of robotic mechanisms," *The international journal of Robotics Research*, vol. 4, no. 2, pp. 3–9, 1985.
- [4] C. Rubert, B. León, A. Morales, and J. Sancho-Bru, "Characterisation of grasp quality metrics," *Journal of Intelligent & Robotic Systems*, vol. 89, pp. 319–342, 2018.
- [5] H. Mnyussiwalla, P. Seguin, P. Vulliez, and J.-P. Gazeau, "Evaluation and selection of grasp quality criteria for dexterous manipulation," *Journal of Intelligent & Robotic Systems*, vol. 104, no. 2, p. 20, 2022.
- [6] R. Krug, Y. Bekiroglu, and M. A. Roa, "Grasp quality evaluation done right: How assumed contact force bounds affect wrench-based quality metrics," in *IEEE Int. Conf. Robot. & Autom. (ICRA)*, 2017.
- [7] M. Haas-Heger, G. Iyengar, and M. Ciocarlie, "Passive reaction analysis for grasp stability," *Transactions on Automation Science and Engineering*, vol. 15, no. 3, pp. 955–966, 2018.
- [8] M. Pozzi, A. M. Sundaram, M. Malvezzi, D. Prattichizzo, and M. A. Roa, "Grasp quality evaluation in underactuated robotic hands," in *IEEE/RSJ Int. Conf. on Intellig. Robots & Systems (IROS)*, 2016.
- [9] D. Prattichizzo, J. K. Salisbury, and A. Bicchi, "Contact and grasp robustness measures: Analysis and experiments," in *Experimental Robotics IV: The 4th Int. Symp., Stanford*, Springer, 1997.
- [10] J. L. Fu and N. S. Pollard, "On the importance of asymmetries in grasp quality metrics for tendon driven hands," in *IEEE/RSJ International Conference on Intelligent Robots and Systems*, 2006.
- [11] J. M. Inouye and F. J. Valero-Cuevas, "Anthropomorphic tendon-driven robotic hands can exceed human grasping capabilities following optimization," *The International Journal of Robotics Research*, vol. 33, no. 5, pp. 694–705, 2014.
- [12] H. Basumatary and S. M. Hazarika, "Design optimization of an underactuated tendon-driven anthropomorphic hand based on grasp quality measures," *Robotica*, vol. 40, no. 11, pp. 4056–4075, 2022.
- [13] I. Llop-Harillo, A. Pérez-González, J. Starke, and T. Asfour, "The anthropomorphic hand assessment protocol (ahap)," *Robotics and Autonomous Systems*, vol. 121, p. 103259, 2019.
- [14] J. Zhou, Y. Chen, D. C. F. Li, Y. Gao, Y. Li, S. S. Cheng, F. Chen, and Y. Liu, "50 benchmarks for anthropomorphic hand function-based dexterity classification and kinematics-based hand design," in *IEEE/RSJ Int. Conf. on Intellig. Robots & Systems (IROS)*, 2020.
- [15] P. Song, J. A. C. Ramón, and Y. Mezouar, "Dynamic evaluation of deformable object grasping," *IEEE Robotics and Automation Letters*, vol. 7, no. 2, pp. 4392–4399, 2022.
- [16] K. Hang, M. Li, J. A. Stork, Y. Bekiroglu, F. T. Pokorny, A. Billard, and D. Kragic, "Hierarchical fingertip space: A unified framework for grasp planning and in-hand grasp adaptation," *IEEE Transactions on robotics*, vol. 32, no. 4, pp. 960–972, 2016.
- [17] J. Inouye and F. J. Valero-Cuevas, "Asymmetric routings with fewer tendons can offer both flexible endpoint stiffness control and high force-production capabilities in robotic fingers," in *IEEE RAS & EMBS International Conference on Biomedical Robotics and Biomechanics*, 2012, pp. 1273–1280.
- [18] N. Vahrenkamp and T. Asfour, "Representing the robot's workspace through constrained manipulability analysis," *Autonomous Robots*, vol. 38, pp. 17–30, 2015.
- [19] N. Vahrenkamp, T. Asfour, and R. Dillmann, "Robot placement based on reachability inversion," in *IEEE International Conference on Robotics and Automation*, 2013, pp. 1970–1975.
- [20] N. Vahrenkamp, E. Kuhn, T. Asfour, and R. Dillmann, "Planning multi-robot grasping motions," in *IEEE-RAS Humanoids*, 2010.
- [21] L. F. Figueredo, R. C. Aguiar, L. Chen, S. Chakrabarty, M. R. Dogar, and A. G. Cohn, "Human comfortability: Integrating ergonomics and muscular-informed metrics for manipulability analysis during human-robot collaboration," *IEEE Robotics and Automation Letters*, vol. 6, no. 2, pp. 351–358, 2020.
- [22] W. S. You, Y. H. Lee, G. Kang, H. S. Oh, J. K. Seo, and H. R. Choi, "Kinematic design optimization for anthropomorphic robot hand based on interactivity of fingers," *Intelligent Service Robotics*, vol. 12, pp. 197–208, 2019.
- [23] O. Khatib, "A unified approach for motion and force control of robot manipulators: The operational space formulation," *IEEE Journal on Robotics and Automation*, vol. 3, no. 1, pp. 43–53, 1987.
- [24] M. Azad, J. Babič, and M. Mistry, "Effects of the weighting matrix on dynamic manipulability of robots," *Autonomous Robots*, vol. 43, no. 7, pp. 1867–1879, 2019.
- [25] A. Ajoudani, N. G. Tsagarakis, and A. Bicchi, "Choosing poses for force and stiffness control," *IEEE Transactions on Robotics*, vol. 33, no. 6, pp. 1483–1490, 2017.
- [26] T. J. Graettinger and B. H. Krogh, "The acceleration radius: A global performance measure for robotic manipulators," *IEEE Journal on Robotics and Automation*, vol. 4, no. 1, pp. 60–69, 1988.
- [27] S. Robotics, "Shadow dexterous hand technical specifications," *Shadow Robot Company, London*. <http://www.shadowrobot.com/>, 2013.